International Journal of Solids and Structures 48 (2011) 1525–1533

Contents lists available at ScienceDirect

International Journal of Solids and Structures

journal homepage: www.elsevier.com/locate/ijsolstr

Effects of interface contacts on the magneto electro-elastic coupling for fiber reinforced composites

Y. Espinosa-Almeyda [a], J.C. López-Realpozo [a], R. Rodríguez-Ramos [a], J. Bravo-Castillero [a], R. Guinovart-Díaz [a], H. Camacho-Montes [b], F.J. Sabina [c,*,1]

[a] Universidad de La Habana, Facultad de Matemática y Computación, Vedado, Habana 4, CP 10400, Cuba
[b] Instituto de Ingeniería y Tecnología, Universidad Autónoma de Ciudad Juárez, Av. Del Charro 610 Norte Cd. Juárez, Chih 32310, Mexico
[c] Department of Applied Mathematics and Theoretical Physics, Centre for Mathematical Sciences, University of Cambridge, Wilberforce Road, Cambridge CB3 0WA, United Kingdom

ARTICLE INFO

Article history:
Received 20 April 2010
Received in revised form 24 November 2010
Available online 4 February 2011

Keywords:
Fiber composite
Effective properties
Magneto electro elastic
Imperfect contact

ABSTRACT

Imperfect bonding between constituents is studied where displacements, electric and magnetic static potentials are considered to have a jump proportional to the normal component of the mechanical traction, electric displacement and magnetic flux. This condition may model various interface damages or the thin glue layer between two adjacent phases. They are termed as the mechanically compliant, dielectrically weakly capacitance and magnetically weakly inductance at the interface. It is shown that while the more imperfect the interface is, the overall properties become weaker, such as longitudinal shear stiffness, out-of-plane piezoelectric coupling, and magnetoelectric coupling. Out-of-plane piezomagnetic coupling, transverse dielectric permittivity and transverse dielectric permeability exhibit no influence by imperfect bonding. The imperfect interface proposed is mimicked by the springs, capacitors and inductances for the mechanical, electric and magnetic interaction between the phases and are highly sensitive to the interphase properties. The results are compared mainly with the self consistent model reported in the literature and good agreements are shown.

1. Introduction

In the last few years, the interest in magnetoelectric effect (ME) (Landau and Lifshitz, 1960) has increased both theoretically and experimentally in an amazing manner (Grossinger et al., 2008; Petrov et al., 2007a,b; Bichurin et al., 2003a,b). A variety of systems exhibit the ME effect, including single phase (de la Vega Reyes et al., 2007; Fuentes et al., 2006). The highest magnetoelectric coefficients are reported for biphasic composites that based their coupling in the mechanical interaction at contact between a piezoelectric and a magnetostrictive phase (Bichurin et al., 2003a; Lin et al., 2005; Petrov and Srinivasan, 2008). That is why many authors have focused their attention on a piezoelectric-piezomagnetic composite (Nie et al., 2009; Srinivas et al., 2009; Singh et al., 2008). Composite materials based on a variety of phase connections can also be found in the literature including layered structures (Cao et al., 2008; Zhang and Wei, 2008), thin films (Delgado et al., 2009; Guyomar et al., 2009) and nanostructures (Hua et al., 2008; Glinchuk et al., 2008).

In previous works (Camacho-Montes et al., 2006, 2009; Bravo-Castillero et al., 2009) determined analytical expressions for the effective properties of magneto-electro-elastic (MEE) fibrous composite where perfect interface conditions were assumed. Perfect bonding invokes that the displacement and the interfacial traction are continuous across the boundary between the constituents. However, experiments show that local or partial debonding at interfaces is a rule rather than the exception in materials such as reinforced metal matrix composites (Llorca and Gonzales, 1997). This leads to strength degradation and the reduction of the effective stiffness.

Furthermore, heterogeneous smart materials might exhibit new properties not existing in any of the constituents due to the coupling of different fields. For example, the most interesting behavior of fibers composites consisting of piezoelectric and piezomagnetic constituents is that the magneto-electric effect, which is only present in composites but absent in constituent phases, is created by the interaction between the constituent phases, a result of the so-called product property (Nan, 1994). The mechanical constitutive response of the active materials can be coupled with the non-mechanical effects as in Camacho-Montes et al. (2009).

* Corresponding author. Address: Instituto de Investigaciones en Matemáticas Aplicadas y en Sistemas, Universidad Nacional Autónoma de México, Apartado Postal 20-726, Delegación de Alvaro Obregón, 01000 México, D.F., Mexico. Tel.: +44 1223 337 887; fax: +44 1223 765900.
E-mail address: fjs@mym.iimas.unam.mx (F.J. Sabina).
[1] Sabbatical leave (until June 30).

0020-7683/$ - see front matter © 2011 Elsevier Ltd. All rights reserved.
doi:10.1016/j.ijsolstr.2011.01.034

Theoretical studies have also received considerable attention in the search of better understanding and improving the magneto-electric coupling (Fuentes et al., 2007; Petrov et al., 2007a; Corcolle et al., 2008; Tong et al., 2008; Camacho-Montes et al., 2009). However, only recently, the question of the influence of the interface on the magnetoelectric property has been raised (Wang and Pan, 2007). Hence, in the present work, we focused our efforts on the so-called imperfect contact interface under longitudinal shear. Both the fiber and matrix are assumed to be transversely isotropic (6 mm material symmetry about the fiber axis). For a composite whose characteristic length is greater than the lattice cell, the method of asymptotic homogenization yields closed-form expressions for the effective coefficients. The effective coefficients for the antiplane problem by means of the complex variable method are calculated. They are useful to establish benchmarks for numerical studies. The formulae exhibit explicitly the dependence on (i) the geometry through the radius of the cylinders, (ii) the periodicity of the array through its lattice sums, (iii) the influence of the imperfect interface contact under longitudinal shear on the magneto-electroelastic composite, and finally (iv) the material properties of the constituents.

Different approaches on interface defects through jumps in the electric and magnetic potentials may be found in literature such as Gao et al. (2003) and Chang and Carman (2007), multi-coating approach (Koutsawa et al., 2010). The imperfect interface proposed in the present work is a natural extension of the shear lag model (or the spring layer model): (a) tractions are continuous but displacements are discontinuous across the imperfect interface. The jumps in displacement components are further assumed to be proportional, in terms of the "spring-factor-type" interface parameters, to their respective interface traction components; (b) the normal electric displacement is continuous but the electric potential is discontinuous across the interface. The jump in the electric potential is proportional to the normal electric displacement; (c) the normal magnetic flux is continuous but the magnetic potential is discontinuous across the interface. The jump in the magnetic potential is proportional to the normal magnetic flux. This general imperfect interface, which could model various interfacial damages (e.g., debonding, sliding and/or cracking across the interface) and could also simulate the thin glue layer between any two adjacent phases, is termed the mechanically compliant, dielectrically weakly capacitor and magnetically weakly impedance interface. Numerical calculations are carried out for $BaTiO_3/CoFe_2O_4$ composite. The shear modulus experiments stiffening due to the coupling piezoelectric and piezomagnetic effect. The dielectric permittivity and the magnetic permeability are influenced by the coupling effects, but their amplitude leads to very small influences. The magneto-electric (ME) effect results form the mechanical interaction between the phases and are highly sensitive to the interphase properties.

2. Governing equations and interface conditions

A two-phase periodic composite is considered here which consists of a square or hexagonal array of identical parallel circular cylinders embedded in a homogeneous medium. The cylinders are infinitely long. Fig. 1 shows the unit cell in the plane normal to cylindrical axis. The magnetoelectroelastic material properties of each phase belong to the crystal symmetry class 6 mm, where the axes of material and geometric symmetry are parallel. The governing magnetoelectroelastic equations for this kind of material are the Navier equations of linear elasticity for the mechanical displacement $\mathbf{u} = (u, v, w)$ and Maxwell's quasistatic equations for electric field $\mathbf{E} = (E_1, E_2, E_3)$ and magnetic field $\mathbf{H} = (H_1, H_2, H_3)$. They become coupled equations for $\mathbf{u}$, $\mathbf{E}$ and $\mathbf{H}$ through the constitutive relations of the medium. In a two-dimensional situation, like in the considered geometry here, it turns out that the above equations uncouple into two independent systems under suitable boundary conditions. Just like, the familiar plane- and anti-plane-strain deformation states in linear elasticity, see Camacho-Montes et al. (2006, 2009).

One of them involves u; v; E_3, B_3, i.e., it is a state of in-plane mechanical deformation and out-of-plane electric and magnetic fields. The other state, which is of particular interest in this work, is characterized by an out-of-plane mechanical displacement w and an in-plane electric field E_1; E_2 and magnetic field H_1; H_2. The main aim of this paper is the determination of effective properties using the homogenization method, say, as in Camacho-Montes et al. (2009) and Lopez-Lopez et al. (2005), considering mechanical, dielectric and magnetic imperfect conditions at the interfaces. Thus it is only necessary to deal with w; E_1; E_2; H_1; H_2. In this case the relevant constitutive relations are

$$\sigma_{13} = 2p\varepsilon_{13} - sE_1 - qH_1, \tag{1}$$
$$\sigma_{23} = 2p\varepsilon_{23} - sE_2 - qH_2, \tag{2}$$
$$D_1 = 2s\varepsilon_{13} + tE_1 + \alpha H_1, \tag{3}$$
$$D_2 = 2s\varepsilon_{23} + tE_2 + \alpha H_2, \tag{4}$$
$$B_1 = 2q\varepsilon_{13} + \alpha E_1 + \mu H_1, \tag{5}$$
$$B_2 = 2q\varepsilon_{23} + \alpha E_2 + \mu H_2 \tag{6}$$

and $p = c_{1313} = c_{2323}$, $s = e_{113} = e_{223}$, $t = \kappa_{11} = \kappa_{22}$, $q = q_{113} = q_{223}$, $\alpha = \alpha_{11} = \alpha_{22}$, $\mu = \mu_{11} = \mu_{22}$ are the elastic modulus, piezoelectric coefficient, dielectric permittivity, piezomagnetic coefficient, magnetoelectric (ME) coefficient, and the magnetic permeability, respectively. Note the differential relations $2\varepsilon_{13} = w_{,1}$, $2\varepsilon_{23} = w_{,2}$, $E_1 = -\phi_{,1}, E_2 = -\phi_{,2}, H_1 = -\psi_{,1}, H_2 = -\psi_{,2}$ where ϕ and ψ are the electric and magnetic potentials; comma notation is understood to denote differentiation with respect to x_i.

Two distinct phases, occupying S_1 and S_2 (Figs. 1 and 2) are assumed to be in perfect contact along the interface of each cylinder

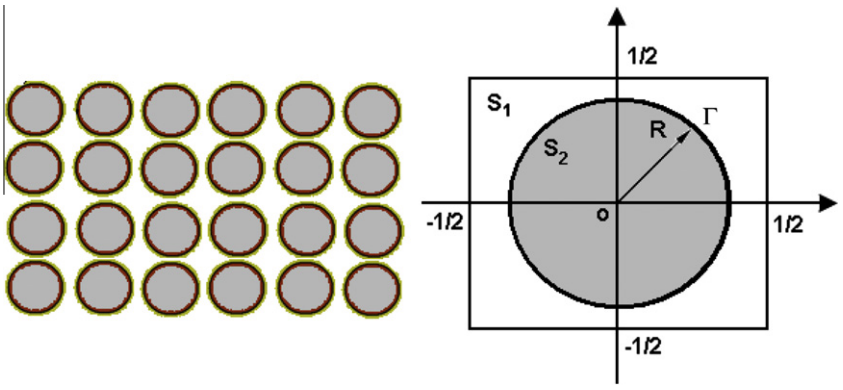

Fig. 1. Transverse section of fiber periodic composite with imperfect interface contacts and square periodic cell.

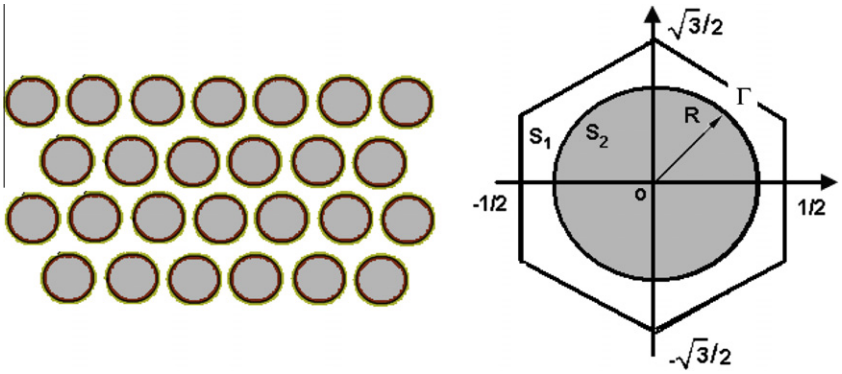

Fig. 2. Transverse section of fiber periodic composite with imperfect interface contacts and hexagonal periodic cell.

which is denoted by Γ. In order to model various possible damages occurring on the fiber–matrix interface and to simulate the thin glue layer existing between two adjacent phases, we adopt the following generalized shear lag model as in Wang and Pan (2007) and Shodja et al. (2007), which can be teamed as the mechanically compliant, dielectrically and magnetically weakly conducting interface

$$\begin{aligned}\sigma_{\beta 3}^{(\gamma)} &= (-1)^{\gamma+1}\widehat{K}\,\|w\|,\\ D_{\beta}^{(\gamma)} &= (-1)^{\gamma}\widehat{M}\,\|\varphi\|,\\ B_{\beta}^{(\gamma)} &= (-1)^{\gamma}\widehat{N}\,\|\psi\|, \quad (\beta,\gamma=1,2).\end{aligned} \tag{7}$$

The double bar notation is used to denote the jump of the relevant function across the interphase taken from the matrix S_1 to the fiber S_2. By definition $\|f\| = f^{(1)} - f^{(2)}$ and $\widehat{K},\widehat{M}$ and $\widehat{N}$ are non negative parameters, $\widehat{K}$ has dimensions of stress, $\widehat{M}$ of electric displacement and $\widehat{N}$ of magnetic induction. Perfect interface (Camacho-Montes et al., 2009) corresponds to case where $\widehat{K},\widehat{M},\widehat{N}\to\infty$. The case $\widehat{K}=\widehat{M}=\widehat{N}=0$ corresponds to the total debond and charge-free interface.

3. Method of solution

Let l be the distance between the centers of two neighboring cylinders and L the diameter of the composite. Then, when l/L is a very small number, it is possible to distinguish two spatial scales, one is x, the slow variable, and the other is $y = x/\varepsilon$, the fast variable. Substituting matrix and fiber constitutive relations (1)–(6) into Navier and Maxwell's equations, inhomogeneous governing equations arise for the herein studied composite (Fig. 1) that can be solved asymptotically posing the ansatz:

$$w(x) = w_0(x,y) + \varepsilon w_1(x,y) + O(\varepsilon^2), \tag{8}$$

$$\varphi(x) = \varphi_0(x,y) + \varepsilon\varphi_1(x,y) + O(\varepsilon^2), \tag{9}$$

$$\psi(x) = \psi_0(x,y) + \varepsilon\psi_1(x,y) + O(\varepsilon^2) \tag{10}$$

and using the method of two scales. The functions w_i, φ_i, $(i = 0,1,)$ are found to satisfy certain differential equations related to the original system in a unit cell (see Fig. 1) with periodic conditions. It is a well-known derivation whose details can be found elsewhere (e.g., Parton and Kudryavtsev, 1993) and here is omitted. Of a greater interest are the so-called local (or canonical) problems associated here with the correction terms w_1, φ_1 and ψ_1 to the mean variations w_0, φ_0 and ψ_0, respectively, since they appear in the formulae of the effective properties. There are six of such problems, which are referred as ${}_{13}L$, ${}_{23}L$, ${}_{1}L$, ${}_{2}L$, ${}_{1}J$ and ${}_{2}J$. A pre-index is used to distinguish similar constants and functions such as displacements and potentials, which appear below. Due to the linearity of the Eqs. (1)–(6), the corrections terms w_1, φ_1 and ψ_1 can be obtained as a linear combination of some of such displacements and potentials. This, however, will not be done here, since the main objective of this paper is the characterization of the six effective properties $\bar{p}$, $\bar{s}$, $\bar{t}$, $\bar{q}$, $\bar{\alpha}$ and $\bar{\mu}$. Due to composite and constitutive symmetries, there are several alternatives for each property: two for $\bar{p}$, $\bar{t}$, $\bar{\alpha}$ and $\bar{\mu}$, four for $\bar{s}$ and $\bar{q}$ as follows,

$$\begin{aligned}\bar{p} &= p_v + \langle {}_{13}p\mathcal{L}_{,1} + {}_{13}s\mathcal{M}_{,1} + {}_{13}q\mathcal{N}_{,1}\rangle\\ &= p_v + \langle {}_{23}p\mathcal{L}_{,2} + {}_{23}s\mathcal{M}_{,2} + {}_{23}q\mathcal{N}_{,2}\rangle,\end{aligned} \tag{11}$$

$$\begin{aligned}\bar{s} &= s_v + \langle {}_{13}s\mathcal{L}_{,1} - {}_{13}t\mathcal{M}_{,1} - {}_{13}\alpha\mathcal{N}_{,1}\rangle\\ &= s_v + \langle {}_{23}s\mathcal{L}_{,2} - {}_{23}t\mathcal{M}_{,2} - {}_{23}\alpha\mathcal{N}_{,2}\rangle\\ &= s_v + \langle {}_{1}p\mathcal{P}_{,1} + {}_{1}s\mathcal{Q}_{,1} + {}_{1}q\mathcal{R}_{,1}\rangle\\ &= s_v + \langle {}_{2}p\mathcal{P}_{,2} + {}_{2}s\mathcal{Q}_{,2} + {}_{2}q\mathcal{R}_{,2}\rangle,\end{aligned} \tag{12}$$

$$\begin{aligned}\bar{q} &= q_v + \langle {}_{13}q\mathcal{L}_{,1} - {}_{13}\alpha\mathcal{M}_{,1} - {}_{13}\mu\mathcal{N}_{,1}\rangle\\ &= q_v + \langle {}_{23}q\mathcal{L}_{,2} - {}_{23}\alpha\mathcal{M}_{,2} - {}_{23}\mu\mathcal{N}_{,2}\rangle\\ &= q_v + \langle {}_{1}p\mathcal{S}_{,1} + {}_{1}s\mathcal{T}_{,1} + {}_{1}q\mathcal{V}_{,1}\rangle\\ &= q_v + \langle {}_{2}p\mathcal{S}_{,2} + {}_{2}s\mathcal{T}_{,2} + {}_{2}q\mathcal{V}_{,2}\rangle,\end{aligned} \tag{13}$$

$$\begin{aligned}\bar{t} &= t_v - \langle {}_{1}s\mathcal{P}_{,1} - {}_{1}t\mathcal{Q}_{,1} - {}_{1}\alpha\mathcal{R}_{,1}\rangle\\ &= t_v - \langle {}_{2}s\mathcal{P}_{,2} - {}_{2}t\mathcal{Q}_{,2} - {}_{2}\alpha\mathcal{R}_{,2}\rangle,\end{aligned} \tag{14}$$

$$\begin{aligned}\bar{\mu} &= \mu_v - \langle {}_{1}q\mathcal{S}_{,1} - {}_{1}\alpha\mathcal{T}_{,1} - {}_{1}\mu\mathcal{V}_{,1}\rangle\\ &= \mu_v - \langle {}_{2}q\mathcal{S}_{,2} - {}_{2}\alpha\mathcal{T}_{,2} - {}_{2}\mu\mathcal{V}_{,2}\rangle,\end{aligned} \tag{15}$$

$$\begin{aligned}\bar{\alpha} &= \alpha_v - \langle {}_{1}q\mathcal{P}_{,1} - {}_{1}\alpha\mathcal{Q}_{,1} - {}_{1}\mu\mathcal{R}_{,1}\rangle\\ &= \alpha_v - \langle {}_{2}qP_{,2} - {}_{2}\alpha\mathcal{Q}_{,2} - {}_{2}\mu\mathcal{R}_{,2}\rangle\\ &= \alpha_v - \langle {}_{1}s\mathcal{S}_{,1} - {}_{1}t\mathcal{T}_{,1} - {}_{1}\alpha\mathcal{V}_{,1}\rangle\\ &= \alpha_v - \langle {}_{2}s\mathcal{S}_{,2} - {}_{2}t\mathcal{T}_{,2} - {}_{2}\alpha\mathcal{V}_{,2}\rangle,\end{aligned} \tag{16}$$

where the italics symbols denote double periodic functions, solutions of the local problems. The functions $\mathcal{L},\mathcal{M}$ and $\mathcal{N}$ of variable $z = y_1 + iy_2$ (Fig. 1) are solutions of the local problems ${}_{13}L$ and ${}_{23}L$; in similar manner the functions $\mathcal{P}$, $\mathcal{Q}$ and $\mathcal{R}$ correspond to ${}_{1}L$, ${}_{2}L$; and $\mathcal{S},\mathcal{T}$ and $\mathcal{V}$ to ${}_{1}J$ and ${}_{2}J$.

The subscripts before the material constants are associated to the corresponding local problems, for instance, ${}_{13}p$ or ${}_{23}p$ mean that the effective coefficient is calculated from the local problem ${}_{13}L$ or ${}_{23}L$, respectively. The subscript v refers to the Voigt average or arithmetic mean of the relevant quantity, that is $f_v = (1-V)f^{(1)} + Vf^{(2)}$, where V is the area fractions occupied by the fiber material.

4. Solution of the local problem ${}_{13}L$

The local problem ${}_{13}L$ is now formulated and for clarity the preindices are omitted for the local functions, (in the above equations $L = {}_{13}L$, $p = {}_{13}p$, etc.).

The problem consists of finding the S-periodic $\mathcal{L}, \mathcal{M}$ and $\mathcal{N}$ functions that satisfy the Laplace equations

$$\Delta\mathcal{L}^{(\gamma)} = \Delta\mathcal{M}^{(\gamma)} = \Delta\mathcal{N}^{(\gamma)} = 0 \quad \text{in } S_\gamma \quad \text{regions } (\gamma = 1, 2), \tag{17}$$

which have null average over the cell S, $\langle\mathcal{L}\rangle = \langle\mathcal{M}\rangle = \langle\mathcal{N}\rangle = 0$ and satisfies the following conditions at the interface Γ,

$$\begin{aligned}
&\|p\mathcal{L}_j + s\mathcal{M}_j + q\mathcal{N}_j\|n_j = -\|p\|n_1,\\
&\|s\mathcal{L}_j - t\mathcal{M}_j - \alpha\mathcal{N}_j\|n_j = -\|s\|n_1,\\
&\|q\mathcal{L}_j - \alpha\mathcal{M}_j - \mu\mathcal{N}_j\|n_j = -\|q\|n_1,\\
&\left(p^{(\gamma)}\mathcal{L}_j^{(\gamma)} + s^{(\gamma)}\mathcal{M}_j^{(\gamma)} + q^{(\gamma)}\mathcal{N}_j^{(\gamma)}\right)n_j^{(\gamma)} + p^{(\gamma)}n_1^{(\gamma)} = (-1)^{\gamma+1}\widehat{K}\,\|\mathcal{L}\|,\\
&\left(s^{(\gamma)}\mathcal{L}_j^{(\gamma)} - t^{(\gamma)}\mathcal{M}_j^{(\gamma)} - \alpha^{(\gamma)}\mathcal{N}_j^{(\gamma)}\right)n_j^{(\gamma)} + s^{(\gamma)}n_1^{(\gamma)} = (-1)^{\gamma}\widehat{M}\,\|\mathcal{M}\|,\\
&\left(q^{(\gamma)}\mathcal{L}_j^{(\gamma)} - \alpha^{(\gamma)}\mathcal{M}_j^{(\gamma)} - \mu^{(\gamma)}\mathcal{N}_j^{(\gamma)}\right)n_j^{(\gamma)} + q^{(\gamma)}n_1^{(\gamma)} = (-1)^{\gamma}\widehat{N}\,\|\mathcal{N}\|,\\
&(j = 1, 2).
\end{aligned} \tag{18}$$

Thus, the functions $\mathcal{L}$, $\mathcal{M}$ and $\mathcal{N}$ are sought such that they are doubly periodic harmonic functions of the complex variable $z = y_1 + iy_2$ in the periodic cell $S = S_1 \cup S_2$, with $S_1 \cap S_2 = \emptyset$ of periods $\omega_1 = 1$ and $\omega_2 = e^{i\theta}$ where $\theta = \pi/2$ for square symmetry and $\theta = \pi/3$ for hexagonal symmetry (Figs. 1 and 2).

Doubly periodic harmonic functions are to be found in terms of the following Laurent expansions of harmonic functions over the region S_1,

$$\begin{aligned}
\mathcal{L}^{(1)}(z) &= \mathrm{Re}\left\{a_1\frac{\pi R}{\sin\theta} + \sum_{p=1}^{\infty}{}^{o}a_p\left(\frac{R}{z}\right)^p + \sum_{p=1}^{\infty}{}^{o}\sum_{k=1}^{\infty}{}^{o}a_k\sqrt{\frac{k}{p}}w_{kp}\left(\frac{z}{R}\right)^p\right\},\\
\mathcal{M}^{(1)}(z) &= \mathrm{Re}\left\{b_1\frac{\pi R}{\sin\theta} + \sum_{p=1}^{\infty}{}^{o}b_p\left(\frac{R}{z}\right)^p + \sum_{p=1}^{\infty}{}^{o}\sum_{k=1}^{\infty}{}^{o}b_k\sqrt{\frac{k}{p}}w_{kp}\left(\frac{z}{R}\right)^p\right\},\\
\mathcal{N}^{(1)}(z) &= \mathrm{Re}\left\{c_1\frac{\pi R}{\sin\theta} + \sum_{p=1}^{\infty}{}^{o}c_p\left(\frac{R}{z}\right)^p + \sum_{p=1}^{\infty}{}^{o}\sum_{k=1}^{\infty}{}^{o}c_k\sqrt{\frac{k}{p}}w_{kp}\left(\frac{z}{R}\right)^p\right\}
\end{aligned} \tag{19}$$

and power expansions over the region S_2,

$$\begin{aligned}
\mathcal{L}^{(2)}(z) &= \mathrm{Re}\left\{\sum_{k=1}^{\infty}{}^{o}d_k\left(\frac{z}{R}\right)^k\right\}, \quad \mathcal{M}^{(2)}(z)\\
&= \mathrm{Re}\left\{\sum_{k=1}^{\infty}{}^{o}e_k\left(\frac{z}{R}\right)^k\right\}, \quad \mathcal{N}^{(2)}(z) = \mathrm{Re}\left\{\sum_{k=1}^{\infty}{}^{o}f_k\left(\frac{z}{R}\right)^k\right\},
\end{aligned} \tag{20}$$

where

$$w_{kp} = \frac{(k+p-1)!}{(k-1)!(p-1)!}\frac{R^{k+p}}{\sqrt{kp}}S_{k+p}, \quad k + l > 2,$$

$S_k = \sum_{m,n}(m\omega_1 + n\omega_2)^{-k}$, $m^2 + n^2 \neq 0$, $k \geqslant 3$, by definition $S_2 = 0$,

$a_k, b_k, c_k, d_k, e_k, f_k$ are real undetermined coefficients. The superscript "o" next to the summation symbol means that "k" runs only over odd integers. The first term in each expansion (19) arises due to the quasi-periodicity property of the Zeta function $\varsigma(z)$, which is $\varsigma(z + \omega_\gamma) - \varsigma(z) = \delta_\gamma$, $\delta_1 = \frac{\pi}{\sin\theta}$, $\delta_2 = \delta_1 e^{-i\theta}$.

Eqs. (11)–(16) are easily transformed applying Green's theorem to the area integrals (Camacho-Montes et al., 2009). In particular for the first equalities in (11), (12) and (13) respectively, the doubly periodic boundary conditions on S, the discontinuity of displacement and potentials on Γ and making the transformations in Appendix A, leads to the dimensionless effective properties

$$\begin{aligned}
\bar{p} &= 1 - 2\frac{R\pi}{\sin\theta}(a_1 + b_1E_{15}^{(1)} + c_1Q_{15}^{(1)}),\\
\bar{s} &= E_{15}^{(1)} - 2\frac{R\pi}{\sin\theta}\left(a_1E_{15}^{(1)} - b_1 - c_1A_{11}^{(1)}\right),\\
\bar{q} &= Q_{15}^{(1)} - 2\frac{R\pi}{\sin\theta}\left(a_1Q_{15}^{(1)} - b_1A_{11}^{(1)} - c_1\right),
\end{aligned} \tag{21}$$

where the coefficients $E_{15}^{(1)}, Q_{15}^{(1)}$ and $A_{11}^{(1)}$ are defined in Appendix A.

In order to obtain the constants a_1, b_1 and c_1, it is necessary to solve the following system of equations, obtained by the combinations of (18)–(20) and written in the following non-dimensional form as

$$\begin{aligned}
&\left(\begin{pmatrix}\beta_{1p} & \alpha_{1p} & \gamma_{1p}\\ \beta_{3p} & \alpha_{3p} & \gamma_{3p}\\ \beta_{5p} & \alpha_{5p} & \gamma_{5p}\end{pmatrix} + \delta_{1p}V\begin{pmatrix}\beta_{2p} & \alpha_{2p} & \gamma_{2p}\\ \beta_{4p} & \alpha_{4p} & \gamma_{4p}\\ \beta_{6p} & \alpha_{6p} & \gamma_{6p}\end{pmatrix}\right)\begin{pmatrix}a_p\\ b_p\\ c_p\end{pmatrix}\\
&\quad + \left[\begin{pmatrix}\beta_{2p} & \alpha_{2p} & \gamma_{2p}\\ \beta_{4p} & \alpha_{4p} & \gamma_{4p}\\ \beta_{6p} & \alpha_{6p} & \gamma_{6p}\end{pmatrix}w_{kp}\begin{pmatrix}a_k\\ b_k\\ e_k\end{pmatrix}\right] = R\begin{pmatrix}\lambda_1\\ \lambda_2\\ \lambda_3\end{pmatrix}\delta_{1p},
\end{aligned} \tag{22}$$

where the sum by the repeated indices k and p are applied, with k, $p = 1, 3, 5, \ldots$, δ_{1p} is the Kronecker's delta, the constants β_{ip}, α_{ip}, γ_{ip} and λ_i are defined in Appendix B.

From (22) a very important first approximation is obtained if we consider $a_k = b_k = c_k = 0$, $k \geqslant 3$, in this case the unknowns with subscript $p = 1$ survive. It is easily solved and its solution is

$$\begin{pmatrix}a_1\\ b_1\\ e_1\end{pmatrix} = R\left(\begin{pmatrix}\beta_{11} & \alpha_{11} & \gamma_{11}\\ \beta_{31} & \alpha_{31} & \gamma_{31}\\ \beta_{51} & \alpha_{51} & \gamma_{51}\end{pmatrix} + V_2\begin{pmatrix}\beta_{21} & \alpha_{21} & \gamma_{21}\\ \beta_{41} & \alpha_{41} & \gamma_{41}\\ \beta_{61} & \alpha_{61} & \gamma_{61}\end{pmatrix}\right)^{-1}\begin{pmatrix}\lambda_1\\ \lambda_2\\ \lambda_3\end{pmatrix}, \tag{23}$$

The system (22) can be solved for a_1, b_1 and c_1 in closed form. These constants are the basis of the effective coefficients as given in (21), (24) and (25).

The same method used for solving the local problem ${}_{13}L$ may be developed to solve the other anti-plane shear local problems. To have the remaining effective properties, it will only necessary to solve ${}_1L$ and ${}_1J$. These problems are very similar to ${}_{13}L$. They can also be transformed into the same systems of Eq. (22), except that the inhomogeneous terms $(\lambda_1, \lambda_2, \lambda_3)^T$ are different (see Appendix B).

The expression given in (21) provides us the effective dimensionless properties $\bar{p}, \bar{s}$ and $\bar{q}$. From the local problems ${}_1L$ and ${}_1J$ the following dimensionless effective properties are obtained,

$$\begin{aligned}
\bar{s} &= E_{15}^{(1)} - 2\frac{R\pi}{\sin\theta}\left(a_1 + b_1E_{15}^{(1)} + c_1Q_{15}^{(1)}\right),\\
\bar{t} &= 1 + 2\frac{R\pi}{\sin\theta}\left(a_1E_{15}^{(1)} - b_1 - c_1A_{11}^{(1)}\right),\\
\bar{\alpha} &= A_{11}^{(1)} + 2\frac{R\pi}{\sin\theta}\left(a_1Q_{15}^{(1)} - b_1A_{11}^{(1)} - c_1\right)
\end{aligned} \tag{24}$$

for the problem ${}_1L$ and

$$\begin{aligned}
\bar{q} &= Q_{15}^{(1)} - 2\frac{R\pi}{\sin\theta}\left(a_1 + b_1E_{15}^{(1)} + c_1Q_{15}^{(1)}\right),\\
\bar{\alpha} &= A_{11}^{(1)} + 2\frac{R\pi}{\sin\theta}\left(a_1E_{15}^{(1)} - b_1 - c_1A_{11}^{(1)}\right),\\
\bar{\mu} &= 1 + 2\frac{R\pi}{\sin\theta}\left(a_1Q_{15}^{(1)} - b_1A_{11}^{(1)} - c_1\right)
\end{aligned} \tag{25}$$

for the problem ${}_1J$.

The unknowns a_1, b_1 and c_1 are different for each individual local problem. They are obtained from the system (22) taking the corresponding independent terms $(\lambda_1, \lambda_2, \lambda_3)^T$ in Appendix B. The dimensionless effective properties from (21), (24) and (25) are calculated with the coefficients of Appendix B for the matrix

properties. The dimensions can be retrieved using the transformations of Appendix A in the inverse form, i.e.,

$$p = \bar{p}p^{(1)}, \quad t = \bar{t}t^{(1)}, \quad \mu = \bar{\mu}\mu^{(1)}, \quad s = \bar{s}\sqrt{p^{(1)}t^{(1)}},$$
$$q = \bar{q}\sqrt{p^{(1)}\mu^{(1)}} \quad \text{and} \quad \alpha = \bar{\alpha}\sqrt{t^{(1)}\mu^{(1)}}. \tag{26}$$

5. Numerical results

In order to validate the present model, we use the numerical intervals for the dimensionless imperfect parameters K, M, N considered by Wang and Pan (2007). These intervals for proportionality factors run from: 1 to 50 for the mechanical coefficient K, 1 to 250 for the electric one M and 1 to 10^{10} for the magnetic one N.

(1) An important result is that approach in (23) reproduces exactly the values that are determined by Mori–Tanaka self-consistent method reported in Wang and Pan (2007), (see Figs. 2–8).
(2) Numerical simulations are conducted for two phase composite with a $CoFe_2O_4$(Cobalt Ferrite) matrix reinforced by fibers made of $BaTiO_3$ (Barium Titanate) with imperfect bonding. Table 1 shows the constitutive properties (see Wang and Pan, 2007). The effective properties related to the antiplane behavior of the two phase magneto-electro-elastic fibrous composite as function of the fiber volume fraction are studied here in. The aforementioned global properties have been calculated using the asymptotic homogenization method (AHM) described in this work and the method presented by Wang and Pan (2007).

Hexagonal and square periodic fiber arrays can be considered by the AHM where an infinite algebraic system of equations is derived. Numerical results are obtained truncating it until N_0 number of equations. Wang and Pan (2007) derived a general expression for the effective coefficients in a matrix form using the self consistent scheme of Mori and Tanaka (MT) for random fiber distribution.

Figs. 3–8 illustrate the effective parameters p, s, α, t, q, μ and show the excellent coincidence between both models in the whole

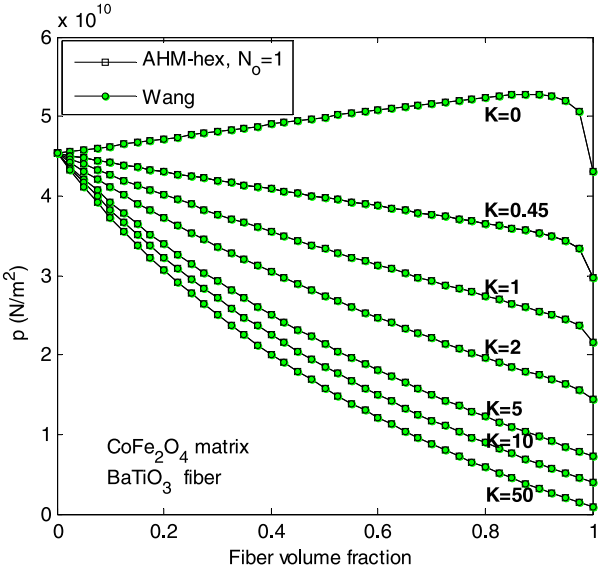

Fig. 3. Comparison between AHM hexagonal array denoted in the present model by AHM-hex and self consistent scheme reported in Wang and Pan (2007) for the variation of the shear elastic effective coefficient p vs volume fraction V_2 of $BaTiO_3$. The two models are coincident for different interfacial mechanic imperfections, characterized by a dimensionless parameter K.

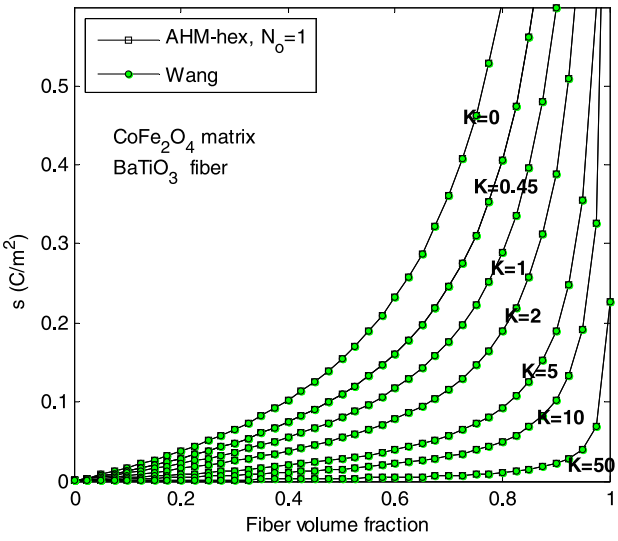

Fig. 4. Variation of the piezoelectric effective coefficient $s = e_{15}$ vs volume fraction V_2 of $BaTiO_3$.

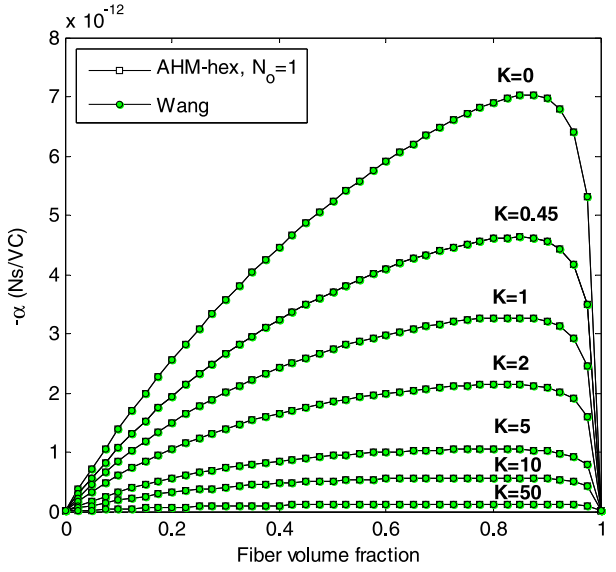

Fig. 5. Variation of the magneto electric effective coefficient vs volume fraction V_2 of $BaTiO_3$.

range of fiber volume fraction. In these figures, Eq. (24) is used to numerically simulate overall properties considering $No = 1$. The effective properties p, s and α become weaker in comparison with perfect contact ($K = 0$) as a consequence of the imperfectly bonded matrix with fibers. They become even weaker with the increase of the K parameter (Figs. 3–5). For the $CoFe_2O_4$ *matrix*/$BaTiO_3$ fiber composite with perfect electric and magnetic phase adhesions, the piezomagnetic coupling q, dielectric permittivity t and magnetic permeability μ effective properties are not affected by the mechanical imperfection and this fact is reflected by both theoretical models (Figs. 6–8).

(2) AHM may be used to further investigate the effect of imperfect bonding considering the six possible combinations resulting from taking into account one type of the three imperfections (elastic, dielectric and magnetic) for the two possible matrix-fiber combinations with $CoFe_2O_4$ and $BaTiO_3$ constituents. The six resulting cases are summarized in Table 2. For each case, the overall properties are divided in two groups: (i) those properties which get weaker because of the imperfection and (ii) those which are not

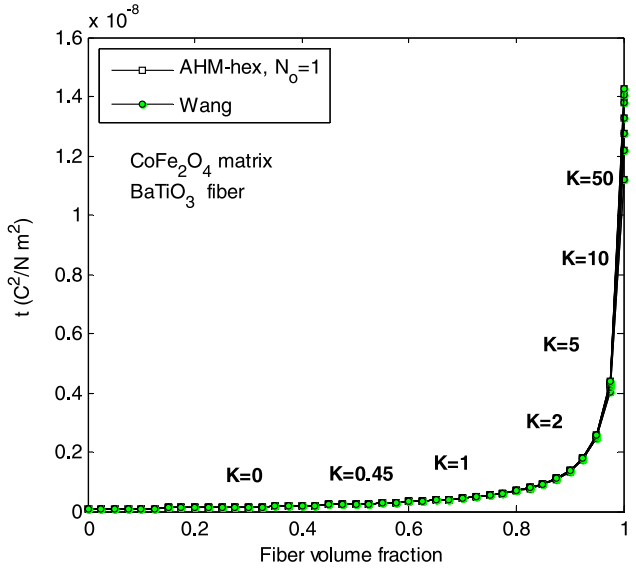

Fig. 6. Variation of the dielectric effective coefficient t vs volume fraction V_2 of $BaTiO_3$. A weak influence of the interfacial imperfections is observed.

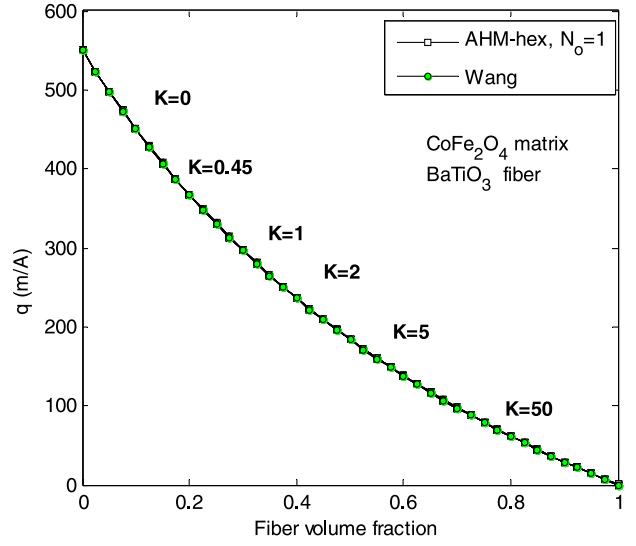

Fig. 7. Variation of the piezomagnetic effective property q vs volume fraction V_2 of $BaTiO_3$. No influence of the imperfect adhesion.

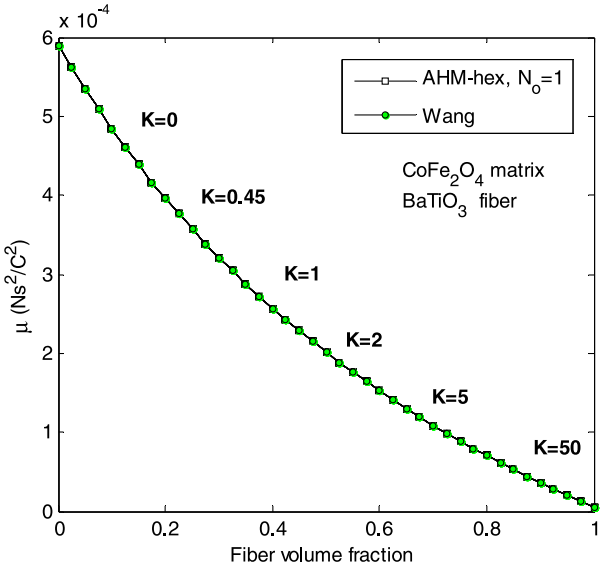

Fig. 8. Variation of the magnetic permeability effective vs volume fraction V_2 of $BaTiO_3$.

Table 1
Material properties of the used constituents in numerical simulations.

	p (Gpa)	s (C/m^2)	q (N/Am)	t ($\times 10^{-9}$C^2/N m^2)	μ ($\times 10^{-6}$N s^2/C^2)
$CoFe_2O_4$	45.3	0	550	0.08	590
$BaTiO_3$	43	11.6	0	11.2	5.0
$BaTiO_3$[a]	43.86	11.4	0	12.8	5.0

[a] Porous material.

Table 2
Summary of the effect of imperfect parameters in the overall properties of the composites. Magneto electric coefficient is affected by all imperfect considerations.

Type of imperfections	$CoFe_2O_4$ matrix, $BaTiO_3$ fiber		$BaTiO_3$ matrix, $CoFe_2O_4$ fiber	
	Influence	No influence	Influence	No influence
Elastic	α, p, s	t, μ, q	α, p, q	s, μ, t
Dielectric	α, t, s	p, μ, q	α	p, s, t, q, μ
Magnetic	α	p, s, t, q, μ	α, q, μ	p, s, i

affected. They are named as "Influence" and "No Influence", respectively. Hence, Table 2 has a practical use to find out whether a type of imperfection has some influence or not on each effective property.

Several interesting conclusions can be stated from Table 2. Here, few of them deserved to be highlighted: (i) the magneto-electric coupling always get weaker with any type of imperfection and any constituent combination, (ii) the coupling property of the matrix (piezoelectric or piezomagnetic) is never affected by the imperfect contact at the overall level, (iii) the coupling property of the fiber gets weaker at the overall level only if the imperfect bonding is related to one of the coupled fields. For example, effective piezoelectricity for a composite with piezoelectric fiber is only affected if the imperfection is either elastic or dielectric, (iv) the stiffness, p, only gets weaker for the imperfect elastic bonding.

Table 2 may offer important tips for composite manufacturing. For instance, when the two phase bonding may be glue with a set of options for its mechanical, dielectric and/or magnetic properties, the weakening bonding effect can be minimized according to the overall property of interest. In general, composite manufacturing parameters must be related to the type of imperfection (K,M, and N) and the affected effective properties.

(3) In Fig. 9 different curves of the α (ME) coefficient are displayed for different values of the electric imperfection M ($M = 0, 10, 50, 250$); $M = 0$ corresponds to the non imperfection case. A comparison between Wang and Pan's model (MT) and the present model are displayed, where the system (22) is truncated to the order $N_0 = 20$. In each case, a maximum value of α is reached and it diminishes as the imperfection parameter M increases. In addition, the maximum for α is shifted to the left for fiber volume fraction with the increase of M. This result is analogous to those reported by Wang and Pan (2007). Fig. 9 also shows that there is an exact coincidence between the AHM for $N_0 = 20$ and the MT scheme until fiber volume fraction near 0.785, higher values exhibits an increasing discrepancy. On the other side, a better coincidence may be found between AHM ($N_0 = 20$).

Also, Fig. 9 shows the α (ME) coefficient for a composite with square periodic cell up to the percolation limit. In the composites where the fibers are aligned with square periodicity, the α property

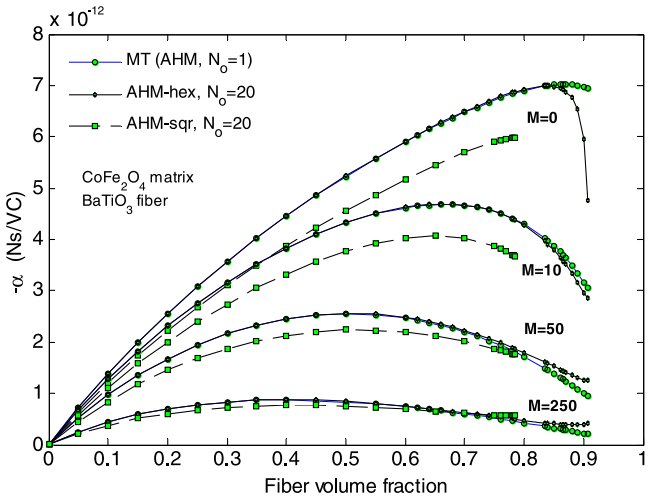

Fig. 9. Variation of the magnetoelectric effective coefficient vs volume fraction V_2 of $BaTiO_3$, calculated by self consistent scheme, AHM hexagonal and AHM square symmetry. The interfacial electric imperfections are characterized by the dimensionless parameter M. The square symmetry presents a weaker behavior.

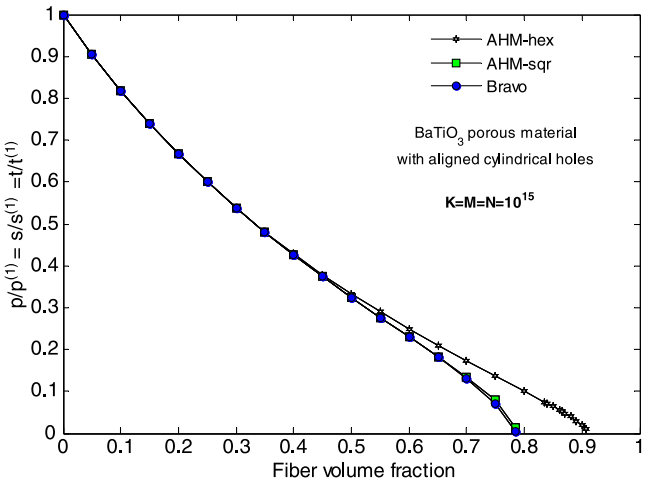

Fig. 11. The total imperfection is characterized by the combination of three parameters K, M and N. The normalized effective axial properties of the composite with empty fibers are obtained.

is weaker than the composites with hexagonal or random distribution even for perfect contact ($M = 0$). In this sense, AHM can be more precise than the result derived from the model of Wang and Pan (2007). AHM shows: (i) Differences that may reach 15%–20% between both square and hexagonal arrays near the maximum for magnetoelectric coupling. (ii) Hexagonal array is quite good to describe random fiber distribution.

AHM for perfect contact makes a correction for the maximum values of α and its fiber volume fraction. The Wang and Pan's model for a composite consisting of $CoFe_2O_4$ matrix reinforced by $BaTiO_3$ fibers reported the maximum value $|\alpha| = 7.03 \times 10^{-12}$ Ns/V C for $V = 0.866$, whereas the present model (AHM hex, with $N_0 = 20$) the maximum value is $|\alpha| = 6.99 \times 10^{-12}$ Ns/V C for $V = 0.835$, which is better adjusted to the homogenization model reported in Fig. 7 by Aboudi (Fig. 7 in Aboudi (2001)) for the perfect contact.

(4) In the above examples, the types of imperfect bonding have been studied separately. Of course, it may be seen as a simplified idealization of composite with imperfect adhesion at the interface. Realistic problems may present several types of imperfect bonding at the same time. The coefficients of the system (22) shown in Appendix B suggest that the combinations of different types of imperfections may be studied as an 'non linear' addition of its effects ($C_1K + C_2M + C_3N$, where $C_i = f(K,M,N)$). Therefore, qualitatively, it may be stated that a superposition results for the consequences of different types of imperfect bonding. Fig. 10 shows the case for the combination of electric and magnetic imperfection. Conclusions of Fig. 10 may be obtained from Fig. 9 and analogous to Fig. 9 for $M = 0$ and $N \neq 0$. Of course, detailed and exact results will require computation with $M \neq 0$ and $N \neq 0$.

(5) The total imperfection is equivalent to obtain the properties of a composite with empty fibers. The properties of empty fiber composites behave as a lower bound related to the properties of a bi-phase composite, with perfect contact conditions. Fig. 11 shows that the analytical herein obtained expressions can effectively describe a porous medium MEE with voids aligned, taking $K = M = N = 10^{15}$ as imperfect parameters. The AHM-sqr curve shows total coincidence with the results reported by Bravo-Castillero et al. (2009) for $BaTiO_3$ porous material.

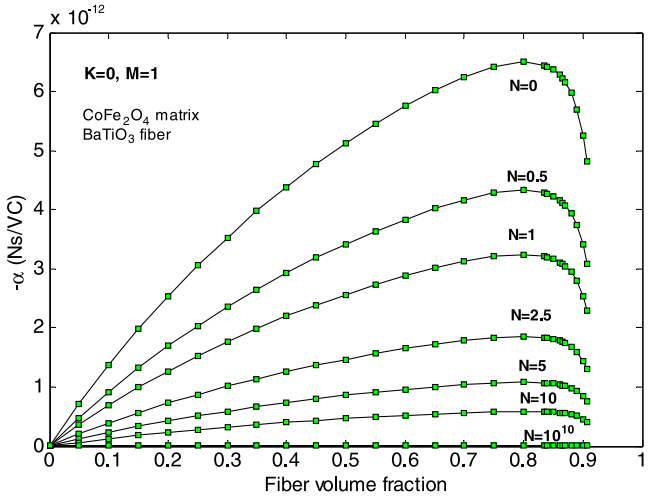

Fig. 10. Variation of magnetoelectric effective coefficient for the combination of electric and magnetic imperfection parameters M and N using AHM-hex.

6. Conclusions

The set of effective properties for a magneto-electro-elastic fiber reinforced composite with imperfect bonding have been obtained by means of the asymptotic homogenization method. For numerical simulations, $CoFe_2O_4$ and $BaTiO_3$ are considered as constituents which can be imperfectly bonded according to a mechanic (K), dielectric (M) and/or magnetic (N) nature. Good coincidence can be observed between AHM results and the Mori Tanaka scheme implemented by Wang and Pan (2007). It is shown that:

1. Magnetoelectric constant always decreases with the increase of K, M or N, i.e., any type of imperfection degrades the magnetoelectric coupling.
2. With the exception of the magnetoelectric overall properties, all the effective properties may be affected depending on the type of imperfection and the nature of the composite constituents. Table 2 summarizes the cases were each overall property is affected or not. Imperfections always induce a decrease in the absolute value of effective properties, if they have some effect on it.

3. The combination of different kinds of imperfections qualitatively induces a superposition of each imperfection separately. However, detailed effect of the imperfection combinations requires calculation that can be easily performed by AHM.
4. For an imperfectly bounded fiber reinforced composite, the case of empty fibers may be used as a lower bound and the perfect bound may be used as upper bound.

Acknowledgements

This work was supported by the Program of Academic Stays 2009. Defects in sensors and dynamic of magnetic-electro-elastic composite. CoNaCyT-México. The funding of Conacyt project number 129658 is gratefully acknowledged. Thanks to Departmento de Matemáticas y Mecánica IIMAS-UNAM for their support and Ramiro Chávez Tovar and Ana Pérez Arteaga for computational assistance. This work was partially written while RRR was visiting the Institute for Interdisciplinary Mathematics (IMI) at Universidad Complutense of Madrid. Thanks to Prof. Miguel Angel Herrero for useful discussions. HCM is also indebted to CoNaCyT grant 100559. FJS thanks the financial support of DGAPA, UNAM.

Appendix A

The local problems (17) and (18) are transformed into dimensionless problems, making the following transformations (Wang and Ding, 2006)

$$E_{15}^{(\gamma)}=\frac{s^{(\gamma)}}{\sqrt{p^{(\gamma)}t^{(\gamma)}}},\quad Q_{15}^{(\gamma)}=\frac{q^{(\gamma)}}{\sqrt{p^{(\gamma)}\mu^{(\gamma)}}},\quad A_{11}^{(\gamma)}=\frac{\alpha^{(\gamma)}}{\sqrt{t^{(\gamma)}\mu^{(\gamma)}}},$$

$$C_{44}^{(\gamma)}=\frac{p^{(\gamma)}}{p^{(\gamma)}}=1,\quad K_{11}^{(\gamma)}=\frac{t^{(\gamma)}}{t^{(\gamma)}}=1,\quad M_{11}^{(\gamma)}=\frac{\mu^{(\gamma)}}{\mu^{(\gamma)}}=1,$$

$$\widehat{\sigma}_{i3}^{(\gamma)}=\frac{\sigma_{i3}^{(\gamma)}}{p^{(\gamma)}},\quad \widehat{D}_{i}^{(\gamma)}=\frac{D_{i}^{(\gamma)}}{\sqrt{p^{(\gamma)}t^{(\gamma)}}},\quad \widehat{B}_{i}^{(\gamma)}=\frac{B_{i}^{(\gamma)}}{\sqrt{p^{(\gamma)}\mu^{(\gamma)}}},$$

$$\widehat{u}_{3}^{(\gamma)}=\frac{u_{3}^{(\gamma)}}{R};\quad \Phi^{(\gamma)}=\sqrt{\frac{t^{(\gamma)}}{p^{(\gamma)}}}\frac{\varphi^{(\gamma)}}{R};\quad \Psi^{(\gamma)}=\sqrt{\frac{\mu^{(\gamma)}}{p^{(\gamma)}}}\frac{\psi^{(\gamma)}}{R}.$$

Appendix B

The constants of the system (22)

$$\beta_{1p}=1,$$

$$\beta_{2p}=\frac{1-\chi_p(1-Kp)-p\sqrt{\chi_p\chi_t}E_{15}^{(1)}E_{15}^{(2)}M-p\sqrt{\chi_p\chi_\mu}Q_{15}^{(1)}Q_{15}^{(2)}N}{1+\chi_p(1+Kp)-p\sqrt{\chi_p\chi_t}E_{15}^{(1)}E_{15}^{(2)}M-p\sqrt{\chi_p\chi_\mu}Q_{15}^{(1)}Q_{15}^{(2)}N},$$

$$\alpha_{1p}=\frac{E_{15}^{(1)}+\chi_pE_{15}^{(1)}pK+\sqrt{\chi_p\chi_t}E_{15}^{(2)}(1+Mp)+p\sqrt{\chi_p\chi_\mu}A_{11}^{(1)}Q_{15}^{(2)}N}{1+\chi_p(1+Kp)-p\sqrt{\chi_p\chi_t}E_{15}^{(1)}E_{15}^{(2)}M-p\sqrt{\chi_p\chi_\mu}Q_{15}^{(1)}Q_{15}^{(2)}N},$$

$$\alpha_{2p}=\frac{E_{15}^{(1)}+\chi_pE_{15}^{(1)}pK-\sqrt{\chi_p\chi_t}E_{15}^{(2)}(1-Mp)+p\sqrt{\chi_p\chi_\mu}A_{11}^{(1)}Q_{15}^{(2)}N}{1+\chi_p(1+Kp)-p\sqrt{\chi_p\chi_t}E_{15}^{(1)}E_{15}^{(2)}M-p\sqrt{\chi_p\chi_\mu}Q_{15}^{(1)}Q_{15}^{(2)}N},$$

$$\gamma_{1p}=\frac{Q_{15}^{(1)}+\chi_pQ_{15}^{(1)}pK+p\sqrt{\chi_p\chi_t}A_{11}^{(1)}E_{15}^{(2)}M+\sqrt{\chi_p\chi_\mu}Q_{15}^{(2)}(1+Np)}{1+\chi_p(1+Kp)-p\sqrt{\chi_p\chi_t}E_{15}^{(1)}E_{15}^{(2)}M-p\sqrt{\chi_p\chi_\mu}Q_{15}^{(1)}Q_{15}^{(2)}N},$$

$$\gamma_{2p}=\frac{Q_{15}^{(1)}+\chi_pQ_{15}^{(1)}pK+p\sqrt{\chi_p\chi_t}A_{11}^{(1)}E_{15}^{(2)}M-\sqrt{\chi_p\chi_\mu}Q_{15}^{(2)}(1-Np)}{1+\chi_p(1+Kp)-p\sqrt{\chi_p\chi_t}E_{15}^{(1)}E_{15}^{(2)}M-p\sqrt{\chi_p\chi_\mu}Q_{15}^{(1)}Q_{15}^{(2)}N},$$

$$\beta_{3p}=1,$$

$$\beta_{4p}=\frac{E_{15}^{(1)}-\sqrt{\chi_p\chi_t}E_{15}^{(2)}(1-Kp)+p\chi_tE_{15}^{(1)}M+p\sqrt{\chi_t\chi_\mu}Q_{15}^{(1)}A_{11}^{(2)}N}{E_{15}^{(1)}+\sqrt{\chi_p\chi_t}E_{15}^{(2)}(1+Kp)+p\chi_tE_{15}^{(1)}M+p\sqrt{\chi_t\chi_\mu}Q_{15}^{(1)}A_{11}^{(2)}N},$$

$$\alpha_{3p}=\frac{-1+p\sqrt{\chi_p\chi_t}E_{15}^{(1)}E_{15}^{(2)}K-\chi_t(1+Mp)-p\sqrt{\chi_t\chi_\mu}A_{11}^{(1)}A_{11}^{(2)}N}{E_{15}^{(1)}+\sqrt{\chi_p\chi_t}E_{15}^{(2)}(1+Kp)+p\chi_tE_{15}^{(1)}M+p\sqrt{\chi_t\chi_\mu}Q_{15}^{(1)}A_{11}^{(2)}N},$$

$$\alpha_{4p}=\frac{-1+p\sqrt{\chi_p\chi_t}E_{15}^{(1)}E_{15}^{(2)}K+\chi_t(1-Mp)-p\sqrt{\chi_t\chi_\mu}A_{11}^{(1)}A_{11}^{(2)}N}{E_{15}^{(1)}+\sqrt{\chi_p\chi_t}E_{15}^{(2)}(1+Kp)+p\chi_tE_{15}^{(1)}M+p\sqrt{\chi_t\chi_\mu}Q_{15}^{(1)}A_{11}^{(2)}N},$$

$$\gamma_{3p}=\frac{-A_{11}^{(1)}+p\sqrt{\chi_p\chi_t}Q_{15}^{(1)}E_{15}^{(2)}K-p\chi_tA_{11}^{(1)}M-\sqrt{\chi_t\chi_\mu}A_{11}^{(2)}(1+Np)}{E_{15}^{(1)}+\sqrt{\chi_p\chi_t}E_{15}^{(2)}(1+Kp)+p\chi_tE_{15}^{(1)}M+p\sqrt{\chi_t\chi_\mu}Q_{15}^{(1)}A_{11}^{(2)}N},$$

$$\gamma_{4p}=\frac{-A_{11}^{(1)}+p\sqrt{\chi_p\chi_t}Q_{15}^{(1)}E_{15}^{(2)}K-p\chi_tA_{11}^{(1)}M+\sqrt{\chi_t\chi_\mu}A_{11}^{(2)}(1-Np)}{E_{15}^{(1)}+\sqrt{\chi_p\chi_t}E_{15}^{(2)}(1+Kp)+p\chi_tE_{15}^{(1)}M+p\sqrt{\chi_t\chi_\mu}Q_{15}^{(1)}A_{11}^{(2)}N},$$

$$\beta_{5p}=1,$$

$$\beta_{6p}=\frac{Q_{15}^{(1)}-\sqrt{\chi_p\chi_\mu}Q_{15}^{(2)}(1-Kp)+p\sqrt{\chi_t\chi_\mu}E_{15}^{(1)}A_{11}^{(2)}M+p\chi_\mu Q_{15}^{(1)}N}{Q_{15}^{(1)}+\sqrt{\chi_p\chi_\mu}Q_{15}^{(2)}(1+Kp)+p\sqrt{\chi_t\chi_\mu}E_{15}^{(1)}A_{11}^{(2)}M+p\chi_\mu Q_{15}^{(1)}N},$$

$$\alpha_{5p}=\frac{-A_{11}^{(1)}+p\sqrt{\chi_p\chi_\mu}E_{15}^{(1)}Q_{15}^{(2)}K-\sqrt{\chi_t\chi_\mu}A_{11}^{(2)}(1+Mp)-p\chi_\mu A_{11}^{(1)}N}{Q_{15}^{(1)}+\sqrt{\chi_p\chi_\mu}Q_{15}^{(2)}(1+Kp)+p\sqrt{\chi_t\chi_\mu}E_{15}^{(1)}A_{11}^{(2)}M+p\chi_\mu Q_{15}^{(1)}N},$$

$$\alpha_{6p}=\frac{-A_{11}^{(1)}+p\sqrt{\chi_p\chi_\mu}E_{15}^{(1)}Q_{15}^{(2)}K+\sqrt{\chi_t\chi_\mu}A_{11}^{(2)}(1-Mp)-p\chi_\mu A_{11}^{(1)}N}{Q_{15}^{(1)}+\sqrt{\chi_p\chi_\mu}Q_{15}^{(2)}(1+Kp)+p\sqrt{\chi_t\chi_\mu}E_{15}^{(1)}A_{11}^{(2)}M+p\chi_\mu Q_{15}^{(1)}N},$$

$$\gamma_{5p}=\frac{-1+p\sqrt{\chi_p\chi_\mu}Q_{15}^{(1)}Q_{15}^{(2)}K-p\sqrt{\chi_t\chi_\mu}A_{11}^{(1)}A_{11}^{(2)}M-\chi_\mu(1+Np)}{Q_{15}^{(1)}+\sqrt{\chi_p\chi_\mu}Q_{15}^{(2)}(1+Kp)+p\sqrt{\chi_t\chi_\mu}E_{15}^{(1)}A_{11}^{(2)}M+p\chi_\mu Q_{15}^{(1)}N},$$

$$\gamma_{6p}=\frac{-1+p\sqrt{\chi_p\chi_\mu}Q_{15}^{(1)}Q_{15}^{(2)}K-p\sqrt{\chi_t\chi_\mu}A_{11}^{(1)}A_{11}^{(2)}M+\chi_\mu(1-Np)}{Q_{15}^{(1)}+\sqrt{\chi_p\chi_\mu}Q_{15}^{(2)}(1+Kp)+p\sqrt{\chi_t\chi_\mu}E_{15}^{(1)}A_{11}^{(2)}M+p\chi_\mu Q_{15}^{(1)}N},$$

where $\chi_p=p^{(2)}/p^{(1)}$, $\chi_t=t^{(2)}/t^{(1)}$, $\chi_\mu=\mu^{(2)}/\mu^{(1)}$, K, M and N are non negative dimensionless parameters, $K=\frac{p^{(1)}R}{\bar{K}}$, $M=\frac{t^{(1)}R}{\bar{M}}$ and $N=\frac{\mu^{(1)}R}{\bar{N}}$.

The inhomogeneous terms $(\lambda_1,\lambda_2,\lambda_3)^T$ for the local problem ${}_{13}L$, are $\lambda_1=\beta_{21}$, $\lambda_2=\beta_{41}$ and $\lambda_3=\beta_{61}$.

The inhomogeneous terms $(\lambda_1,\lambda_2,\lambda_3)^T$ for the local problem ${}_1L$, are

$$\lambda_1=\frac{E_{15}^{(1)}-\sqrt{\chi_p\chi_t}E_{15}^{(2)}+K\chi_pE_{15}^{(1)}+\sqrt{\chi_p\chi_t}E_{15}^{(2)}M+\sqrt{\chi_p\chi_\mu}A_{11}^{(1)}Q_{15}^{(2)}N}{1+\chi_p(1+K)-\sqrt{\chi_p\chi_t}E_{15}^{(1)}E_{15}^{(2)}M-\sqrt{\chi_p\chi_\mu}Q_{15}^{(1)}Q_{15}^{(2)}N},$$

$$\lambda_2=\frac{-1+\chi_t+\sqrt{\chi_p\chi_t}E_{15}^{(1)}E_{15}^{(2)}K-\chi_tM-\sqrt{\chi_t\chi_\mu}A_{11}^{(1)}A_{11}^{(2)}N}{E_{15}^{(1)}+\sqrt{\chi_p\chi_t}E_{15}^{(2)}(1+K)+\chi_tE_{15}^{(1)}M+\sqrt{\chi_t\chi_\mu}Q_{15}^{(1)}A_{11}^{(2)}N},$$

$$\lambda_3=\frac{-A_{11}^{(1)}+\sqrt{\chi_t\chi_\mu}A_{11}^{(2)}+\sqrt{\chi_p\chi_\mu}E_{15}^{(1)}Q_{15}^{(2)}K-\sqrt{\chi_t\chi_\mu}A_{11}^{(2)}M-\chi_\mu A_{11}^{(1)}N}{Q_{15}^{(1)}+\sqrt{\chi_p\chi_\mu}Q_{15}^{(2)}(1+K)+\sqrt{\chi_t\chi_\mu}E_{15}^{(1)}A_{11}^{(2)}M+\chi_\mu Q_{15}^{(1)}N}.$$

The inhomogeneous terms $(\lambda_1,\lambda_2,\lambda_3)^T$ for the local problem ${}_1J$ are

$$\lambda_1=\frac{Q_{15}^{(1)}-\sqrt{\chi_p\chi_\mu}Q_{15}^{(2)}+K\chi_pQ_{15}^{(1)}+\sqrt{\chi_p\chi_t}A_{11}^{(1)}E_{15}^{(2)}M+\sqrt{\chi_p\chi_\mu}Q_{15}^{(2)}N}{1+\chi_p(1+K)-\sqrt{\chi_p\chi_t}E_{15}^{(1)}E_{15}^{(2)}M-\sqrt{\chi_p\chi_\mu}Q_{15}^{(1)}Q_{15}^{(2)}N},$$

$$\lambda_2 = \frac{-A_{11}^{(1)} + \sqrt{\chi_t\chi_\mu}A_{11}^{(2)} + \sqrt{\chi_p\chi_t}E_{15}^{(2)}Q_{15}^{(1)}K - \chi_t A_{11}^{(2)}M - \sqrt{\chi_t\chi_\mu}A_{11}^{(2)}N}{E_{15}^{(1)} + \sqrt{\chi_p\chi_t}E_{15}^{(2)}(1+K) + \chi_t E_{15}^{(1)}M + \sqrt{\chi_t\chi_\mu}Q_{15}^{(1)}A_{11}^{(2)}N},$$

$$\lambda_3 = \frac{-1 + \chi_\mu + \sqrt{\chi_p\chi_\mu}Q_{15}^{(1)}Q_{15}^{(2)}K - \sqrt{\chi_t\chi_\mu}A_{11}^{(1)}A_{11}^{(2)}M - \chi_\mu N}{Q_{15}^{(1)} + \sqrt{\chi_p\chi_\mu}Q_{15}^{(2)}(1+K) + \sqrt{\chi_t\chi_\mu}E_{15}^{(1)}A_{11}^{(2)}M + \chi_\mu Q_{15}^{(1)}N}.$$

References

Aboudi, J., 2001. Micromechanical analysis of fully coupled electro-magneto-thermo-elastic multiphase composites. Smart Mater. Struct. 10, 867–877.

Bichurin, M.I., Filippov, D.A., Petrov, V.M., Laletsin, V.M., Paddubnaya, N., Srinivasan, G., 2003a. Resonance magnetoelectric effects in layered magnetostrictive-piezoelectric composites. Phys. Rev. B 68, 132408.

Bichurin, M.I., Petrov, V.M., Srinivasan, G., 2003b. Theory of low-frequency magnetoelectric coupling in magnetostrictive-piezoelectric bilayers. Phys. Rev. B 68, 054402.

Bravo-Castillero, J., Rodríguez-Ramos, R., Guinovart-Díaz, R., Sabina, F.J., Aguiar, A.R., Silva, U.P., Gómez-Muñoz, J.L., 2009. Analytical formulae for electromechanical effective properties of 3–1 longitudinally porous piezoelectric materials. Acta Mater. 57, 795–803.

Camacho-Montes, H., Rodríguez-Ramos, R., Bravo-Castillero, J., Guinovart-Díaz, R., Sabina, F.J., 2006. Effective coefficients for two phase magneto-electroelastic fibrous composite with square symmetry cell in plane mechanical displacement and out-of-plane electric and magnetic field case. Integr. Ferroelectr. 83, 49–65.

Camacho-Montes, H., Sabina, F.J., Bravo-Castillero, J., Guinovart-Díaz, R., Rodríguez-Ramos, R., 2009. Magnetoelectric coupling and cross-property connections in a square array of a binary composite. Int. J. Eng. Sci. 47, 294–312.

Cao, H., Zhang, N., Wei, J., 2008. Doping effect on crystal structure of $BaTiO_3$ and magnetoelectric coupling of layered composites $Tb_{1-x}Dy_xFe_{2-y}$–$BaTi_{0.99}M_{0.01}O_{3+\delta}$. J. Alloys Comp.. doi:10.1016/j.jallcom.2008.04.060.

Chang, Ch.M., Carman, G.P., 2007. Modeling shear lag and demagnetization effects in magneto-electric laminate composites. Phys. Rev. B 76, 134116.

Corcolle, R., Daniel, L., Bouillault, F., 2008. Generic formalism for homogenization of coupled behavior: Application to magnetoelectroelastic behavior. Phys. Rev. B 78, 214110.

de la Vega Reyes, C., Fuentes, Ma. E., Fuentes, L., 2007. BiFeO3 Synchrotron radiation structure refinement and magnetoelectric geometry. J. Eur. Ceram. Soc. 27, 3709–3711.

Delgado, E., Ostos, C., Martínez-Sarrión, M.L., Mestres, L., Lederman, D., Prieto, P., 2009. Growth and characterization of BLZT–CFO composite thin films. Mater. Chem. Phys. 113, 702–706.

Fuentes, L., García, M., Bueno, D., Fuentes, M.E., Muñoz, A., 2006. Magnetoelectric effect in $Bi_5Ti_3FeO_{15}$ ceramics obtained by molten salts synthesis. Ferroelectrics 336, 81–89.

Fuentes, M.E., Fuentes, L., Olivera, R., Garcia, M., 2007. Meso- and nano-magnetoelectricity: a review. Rev. Mexicana de Física S53 (1), 21–29.

Gao, C.F., Tong, P., Zhang, T.Y., 2003. Interfacial crack problems in magneto-electroelastic solids. Int. J. Eng. Sci. 41, 2105–2121.

Glinchuk, M.D., Eliseev, E.A., Morozovska, A.N., Blinc, R., 2008. Giant magnetoelectric effect induced by intrinsic surface stress in ferroic nanorods. Phys. Rev. B 77, 024106.

Grossinger, R., Duong, G.V., Sato-Turtelli, R., 2008. The physics of magnetoelectric composites. J. Magnet. Magn. Mater. 320, 1972–1977.

Guyomar, D., Matei, D.F., Guiffard, B., Le, Q., Belouadah, R., 2009. Magnetoelectricity in polyurethane films loaded with different magnetic particles. Mater. Lett. 63, 611–613.

Hua, Z., Yang, P., Huang, H., Wan, J., Zhong-Zhen, Y., Yang, S., Mu, L., Gu, B., i Du, Y., 2008. Sol–gel template synthesis and characterization of magnetoelectric $CoFe_2O_4$/Pb(Zr0.52Ti0.48)O3 nanotubes. Mater. Chem. Phys. 107, 541–546.

Koutsawa, Y., Biscani, F., Belouettar, S., Nasser, H., Carrera, E., 2010. Multi-coating inhomogeneities approach for the effective thermo-electro-elastic properties of piezoelectric composite materials. Compos. Struct. 92, 964–972.

Landau, L.D., Lifshitz, E.M., 1960. Electrodynamics of Continuous Media. Pergamon, Oxford. p. 119 (translation of Russian edition, 1958).

Lin, Y., Cai, N., Zhai, J., Liu, G., Ce-Wen, N., 2005. Giant magnetoelectric effect in multiferroic laminated composites. Phys. Rev. B 72, 012405.

Llorca, J., Gonzales, C., 1997. Microstructural factors controlling the strength and ductility of particle-reinforced metalmatrix composites. J. Mech. Phys. Sol. 46, 1–28.

Lopez-Lopez, E., Sabina, F.J., Bravo-Castillero, J., Guinovart-Díaz, R., Rodríguez-Ramos, R., 2005. Overall electromechanical properties of a binary composite with 622 symmetry constituents. Antiplane shear piezoelectric state. Int. J. Solids Struct. 42, 5765–5777.

Nan, C.W., 1994. Magnetoelectric effect in composites of piezoelectric and piezomagnetic phases. Phys. Rev. B 50, 6082–6088.

Nie, J., Xu, G., Yang, Y., Cheng, C., 2009. Strong magnetoelectric coupling in v–$BaTiO_3$ composites prepared by molten-salt synthesis method. Mater. Chem. Phys.. doi:10.1016/j.matchemphys.12.011.

Parton, V.Z., Kudryavtsev, B.A., 1993. Engineering Mechanics of Composite Materials. CRC Press, Boca Raton.

Petrov, V.M., Srinivasan, G., 2008. Enhancement of magnetoelectric coupling in functionally graded ferroelectric and ferromagnetic bilayers. Phys. Rev. B 78, 184421.

Petrov, V.M., Srinivasan, G., Bichurin, M.I., Gupta, A., 2007a. Theory of magnetoelectric effects in ferrite piezoelectric nanocomposites. Phys. Rev. B 75, 224407.

Petrov, V.M., Srinivasan, G., Laletsin, U., Bichurin, M.I., Tuskov, D.S., Paddubnaya, N., 2007b. Magnetoelectric effects in porous ferromagnetic-piezoelectric bulk composites: experiment and theory. Phys. Rev. B 75, 174422.

Shodja, H.M., Tabatabaei, S.M., Kamali, M.T., 2007. A piezoelectric medium containing a cylindrical inhomogeneity: role of electric capacitors and mechanical imperfections. Int. J. Solids Struct. 44, 6361–6381.

Singh, A., Pandey, V., Kotnala, R.K., Pandey, D., 2008. Direct evidence for multiferroic magnetoelectric coupling in $0.9BiFeO_3$–$0.1BaTiO_3$. Phys. Rev. Lett. 101, 247602.

Srinivas, A., Gopalan, R., Chandrasekharan, V., 2009. Room temperature multiferroism and magnetoelectric coupling in $BaTiO_3$_$BaFe_{12}O_{19}$ system. Solid State Commun. 149, 367–370.

Tong, Z.H., Lo, S.H., Jiang, C.P., Cheung, Y.K., 2008. An exact solution for the three-phase thermo-electro-magneto-elastic cylinder model and its application to piezoelectric–magnetic fiber composites. Int. J. Solids Struct. 45, 5205–5219.

Wang, H.M., Ding, H.J., 2006. Transient responses of a magneto-electro-elastic hollow sphere for fully coupled spherically symmetric problem. Eur. J. Mech. A/Solids 25, 965–980.

Wang, X., Pan, E., 2007. Magnetoelectric effects in multiferroic fibrous composite with imperfect interface. Phys. Rev. B 76, 214107.

Zhang, N., Wei, J., 2008. Influence of the concentration in Fe-doped $BaTiO_3$ on magnetoelectric couping of layered composites BaTi1_xFexO3–Tb1_yDyyFe2_z. J. Magn. Magn. Mater. 320, 2387–2389.